Published in final edited form as:
Biomaterials. 2008 August ; 29(23): 3298–3305. doi:10.1016/j.biomaterials.2008.04.008.

Peptide Amphiphile Nanostructure-Heparin Interactions and their Relationship to Bioactivity

Kanya Rajangam[1], **Michael S. Arnold**[2], **Mark A. Rocco**[2], and **Samuel I. Stupp**[2,3,4,5*]

1*Department of Biomedical Engineering, Northwestern University, Evanston IL 60208*

2*Department of Materials Science and Engineering, Northwestern University, Evanston IL 60208*

3*Department of Chemistry, Northwestern University, Evanston IL 60208*

4*Institute for BioNanotechnology in Medicine, Northwestern University, Evanston IL 60208*

5*Department of Medicine, Northwestern University, Evanston IL 60208*

Abstract

Heparin-protein interactions are important in many physiological processes, including angiogenesis, the growth of new blood vessels from existing ones. We have previously developed a highly angiogenic self-assembling gel, wherein the self-assembly process is triggered by interactions between heparin and peptide amphiphiles (PAs) with a consensus heparin binding sequence. In this report, this consensus sequence was scrambled and incorporated into a new peptide amphiphile in order to study its importance in heparin interaction and bioactivity. Heparin was able to trigger gel formation of the scrambled peptide amphiphile (SPA). Furthermore, the affinity of the scrambled molecule for heparin was unchanged as shown by isothermal titration calorimetry and high Förster resonance emission transfer efficiency. However, both the mobile fraction and the dissociation rate constant of heparin, using fluorescence recovery after photobleaching, were markedly higher in its interaction with the scrambled molecule implying a weaker association. Importantly, the scrambled peptide amphiphile- heparin gel had significantly less angiogenic bioactivity as shown by decreased tubule formation of sandwiched endothelial cells. Hence, we believe that the presence of the consensus sequence stabilizes the interaction with heparin and is important for the bioactivity of these new materials.

Introduction

Heparan sulfate-like glycosaminoglycans (HSGAGs) are polydisperse, negatively charged biopolymers made up of dimeric repeats of glucosamine and uronic acid with varying degrees of sulfation [1]. HSGAGs are known to interact with proteins in important physiological processes including angiogenesis, the growth of new blood vessels from existing ones [1–4]. Two types of HSGAGs are heparin and heparan sulfate, which are structurally similar but differ in the degree of sulfation, with heparin being more sulfated than heparan [1]. Heparin, which is readily available, is often used to study the interaction of HSGAGs with proteins [5]. This is particularly true in studying angiogenesis. Both HSGAGs have a similar role in angiogenesis by virtue of their ability to activate angiogenic growth factors like fibroblast growth factor-2

*s-stupp@northwestern.edu.

(FGF-2) [6] and vascular endothelial growth factor (VEGF) [7]. In some physiological processes, however, the effect of both biopolymers could be different, for example, heparin binds strongly to antithrombin III, thus inhibiting blood coagulation while heparan sulfate does so to a much lesser degree [1].

There has been interest in learning more about the nature of the important interaction between HSGAGs and proteins. Cardin and Weintraub revealed that the heparin-binding domains in different proteins have similar sequences following the pattern XBBBXXBX or XBBXBX where X stands for a hydrophobic amino acid and B for a basic amino acid [8]. Heparin binding peptides have been studied for therapeutic use acting as heparin delivery agents [9,10] or in solution as possible heparin antagonists by virtue of their ability to bind strongly to heparin [11,12].

We recently reported on a positively charged peptide amphiphile with a consensus Cardin-Weintraub heparin-binding sequence [13]. Its design was based on the structures developed in our laboratory, which form by self-assembly, nanofibers under appropriate conditions of ionic strength [13–17]. These molecules contain peptide sequences capable of forming β sheets and are transformed into strong amphiphiles by linking covalently an alkyl segment to one terminus of the peptide. Furthermore, the nanofibers are known to form networks that give rise to a self-supporting gel. This particular heparin-binding peptide amphiphile (HBPA) consisted of the novel heparin-binding consensus sequence LRKKLGKA attached to palmitic acid by means of a linker peptide sequence of AAAAGGG [13]. We showed that self-assembly and gel formation of the HBPA is triggered by the addition of heparin, a novel strategy in which a polyion screens charges in PAs and nucleates formation of the nanofibers [13]. Further this HBPA-heparin gel was shown to be very efficient at promoting angiogenesis in vivo in a rat corneal assay [13]. We proposed that this high bioactivity was due to the optimal and large surface area presentation of heparin chains bound to nanofibers as an effective mechanism for signaling with growth factors such as FGF- 2. In order to determine the importance of the consensus peptide sequence for heparin binding by the nanostructures and the consequent bioactivity, we synthesized a peptide amphiphile with a scrambled heparin binding sequence. This was done by separating the hydrophobic and basic amino acids of the consensus sequence of HBPA such that the basic amino acids would be near the surface of the nanofiber. In this work we study the interaction between heparin and nanostructures formed by PAs with the scrambled vs. the consensus peptide (SPA vs. HBPA) using isothermal titration calorimetry (ITC), Förster resonance energy transfer (FRET) and fluorescence recovery after photobleaching (FRAP). We also study bioactivity differences among the two nanostructures using a well accepted in vitro angiogenesis assay.

Materials and Methods

The SPA was synthesized using previously reported methods [15]. The peptide was synthesized on a RINK amide resin in an automated solid phase peptide synthesizer (Applied Biosystems-733A) using appropriately protected amino acids (Novabiochem) for standard fluorenylmethoxycarbonyl (Fmoc) chemistry (all reagents from Fisher Scientific unless specified). The N-terminus of the peptide was then capped with palmitic acid using an alkylation reaction with 5 equivalents of palmitic acid, 7.5 equivalents of diisopropylethylamine (DIEA) and 6 equivalents of 2-(1H-Benzotriazole-1-yl)-1,1,3,3-tetramethyluronium hexafluorophosphate (HBTU) in 2:1 dimethylformamide and dichloromethane. The SPA was deprotected and cleaved from the resin using trifluoracetic acid (TFA), water and triisopropylsilane. The TFA was removed by rotary evaporation, and SPA precipitated using cold diethyl ether and then filtered and vacuum dried. We characterized the molecular weight of the SPA by electrospray ionization mass spectrometry (mass 1605.08). The SPA was solubilized in 1 M hydrochloric acid at room temperature for one hour and then

subsequently lyophilized. The SPA was resolubilized at 30 mg/mL concentration at pH 7.4 (unless otherwise specified) in de-ionized water using 1 M sodium hydroxide as needed. The SPA gels were formed by mixing equal volumes of the SPA solution made as described above and gel heparin sodium from porcine intestinal mucosa (Sigma) in concentrations of 20 mg/mL (to obtain a stoichiometry of 1:1.84 for SPA: heparin). Gel formation was also triggered by adding disodium hydrogen phosphate in solution at a concentration of 11 mg/mL or equal amounts of 0.25 M sodium hydroxide to obtain SPA gels of 1.5 w/v %. Heparin, phosphate or sodium hydroxide was scaled down appropriately to maintain stoichiometry whenever lower weight percent gels were prepared.

Heparin-SPA samples were prepared for transmission electron microscopy (TEM) as previously described [15]. A holey carbon coated copper grid was dipped twice in a 1% SPA-heparin gel suspension for 20 s and then stained with phosphotungstic acid (Sigma) at room temperature. TEM micrographs were obtained using a Hitachi 8100 microscope at an accelerating voltage of 200 kV. A Paar Physica MCR300 rheometer with a stainless steel parallel plate of 20 mm was used to perform oscillating rheology experiments. Gels were prepared in situ and the temperature maintained at 22 °C using a Peltier device. A frequency sweep experiment at 3 % strain and a ten-minute wait time was carried out to obtain 17 data points between angular frequencies of 0.1 to 10 rad/s (data obtained at higher frequencies were not reliable). Single factor analysis of variance (ANOVA) was done on an average of three samples to determine the difference in the elastic modulus between SPA-heparin gels and HBPA-heparin gels ($p << 0.01$), SPA-base gels and HBPA-base gels ($p << 0.01$), SPA-heparin gels and SPA-base gels ($p << 0.01$) and finally HBPA heparin gels and HBPA base gels ($p << 0.01$). Isothermal titration calorimetry (Microcal-ITC) was done by titrating heparin in 4 μL aliquots from a stock solution of 101.5 μg/mL solution into a 40.1 μg/mL SPA solution (both solutions in water). Raw data of heat released versus molar ratio were obtained, corrected for background heat of dilution and integrated using the Microcal software to fit a curve for a single type of binding site and to obtain a binding constant as described previously [18]. CD was done on a Jasco J-715 CD spectrometer using a 0.1 cm path length quartz cuvette on four samples- water only, 0.105 mg of SPA, 0.07 mg of heparin and 0.105 mg SPA + 0.07 mg heparin each in 350μl of water. The pH of all samples was 7.

Confocal fluorescent microscopy for FRET was done as described previously [19]. Acceptor photobleaching was carried out on these samples using a Zeiss LSM 510 laser scanning confocal fluorescent microscope. In these experiments, the sample was excited at 405 nm (the donor's excitation wavelength) and 18 images were captured over the wavelength range of 427 to 609 nm (10 nm steps). A small area of the fibers was saturated with light at 488 nm, within the absorption band of fluorescein, effectively bleaching the acceptor for the FRET system. The same area is then imaged as done before the bleaching. FRET efficiency was calculated as previously reported after normalizing for bleaching due to imaging using the formula, efficiency = 1- (peak pre-bleach donor emission / peak post-bleach donor emission) [19]. In this case donor emission at 470 nm, which was its peak emission wavelength, was used to calculate the FRET efficiency ($n= 4–6$, t test assuming samples of unequal variance gave a p value of 0.01 while comparing the SPA system with the control and a p value of 0.02 comparing the HBPA system with the control).

FRAP was done by mixing 0.03 w/v% SPA or HBPA in water solution and 0.02 w/v% in water of fluorescein-heparin (Sigma) solution to obtain gels which were imaged using the laser scanning confocal fluorescent microscope by exciting fluorescein at 488 nm. Multiple spots were irreversibly photobleached by exposing to 100 % 488 nm light and recovery of fluorescence in these areas was monitored by a time series using a low laser intensity of 0.05%. We analyzed the images using the Zeiss imaging software to obtain the fluorescence intensity values at each time point which were plotted after correction for photobleaching due to imaging

and normalized to the initial fluorescence. The mobile or unbound fraction (U) was determined using the formula $U = (F_\infty - F_0)/(F_i - F_0)$, where F_∞ is the final fluorescence in the bleached region, F_0 is the fluorescence in the bleached region just after bleach and F_i is the initial fluorescence in the spot [20]. A simple closed form expression for the Laplace transform of the exact solution to the differential equation was utilized and numerically fit to the experimental data using a non-linear, least squares fitting routine as previously described using MATLAB software program to obtain the D*, k_{on}* and k_{off} [21]. A t test assuming unequal variances was done to determine statistical significance (n= 3–4, p = 0.001 for mobile fraction comparison and p= 0.04 for k_{off} comparison).

Bovine pulmonary artery endothelial cells (bPAEC) were grown in phenol red free Dulbecco's modified Eagle medium with 20% v/v fetal bovine serum, 1% v/v penicillin-streptomycin, 2% v/v l-glutamine and 1 mM each of sodium pyruvate and modified Eagle medium amino acids (the serum was obtained from Hyclone while the media and other additives from Gibco). Cells were used for the experiments at passage 14 or 15. The freeze media was prepared by adding 5% v/v dimethyl sulfoxide (Sigma) to the above media. The cells were grown in cell culture incubators at 37 °C with 5% CO_2. The sandwich gels were made in 8-well chambered cover slip (Nalge Nunc) containers for better microscopic resolution. The first layer of the PA-heparin gels was made by mixing 100 μL of 30 mg/mL of the respective PA in water at pH 7.5 with 100 μL of 20 mg/mL heparin in the above cell culture media with 12.5 ng each (to give a total concentration in the well of 31.25 ng/mL) of FGF-2 and VEGF (both from Peprotech). Subsequently, 750,000 bPAECs were plated per well in culture media and followed up with alternate day media changes in the incubator until they grew in layers through the gel (usually by day 5). The second layer of gel was made on top of the cell layer exactly as before after removing excess media. After a half hour at room temperature, excess media was added and the wells were incubated at 37 °C and with media changes every alternate day. At day 7, the cells were stained with a fluorescein-based cell tracer (Vybrant CFDA SE cell tracer, Molecular Probes) at 20 μM concentration and imaged using a Leica laser confocal scanning microscope (DM IRE2) to obtain a z-series through the gels. Tubule length was quantified after blinding the images by manually tracing lines on them using Metamorph imaging software (supplementary figure 2) on low power images of at least twelve randomly selected areas of each sample. The average tubule length per image was then compared between HBPA heparin gels with growth factors and both types of the SPA heparin gels using a t-test assuming unequal variances ($p << 0.01$). When a similar statistical test was performed between the two types of HBPA heparin gels, the p- values was 0.01.

Results and Discussion

SPA is a linear molecule consisting of a palmitic acid residue as its hydrophobic component with the same amino acid residues as HBPA but a scrambled sequence relative to the consensus peptide, of LLGARKKK (Figure 1). It is soluble in water, and when a dilute aqueous solution of SPA was mixed with a dilute aqueous solution of heparin the molecules self-assembled into nanofibers and a gel was formed. This gel was made up of bundles of nanofibers, as observed by transmission electron microscopy (Figure 2). Nanofiber formation in our PAs is triggered by charge neutralization or screening at an appropriate pH or by the addition of multivalent ions, respectively. This drives the formation of β-sheet association of peptide segments and the hydrophobic collapse of the fatty acid tails into a cylindrical supramolecular aggregate [13–17,22]. In the case of SPA, this effect was also induced by the addition of heparin to a solution of the molecules. This suggests that the sulfated negatively charged biopolymer is effective at screening monomer charges to enable self-assembly in either HBPA or SPA. This is further confirmed by the fact that negatively charged phosphate ions from a solution of disodium hydrogen phosphate or sodium hydroxide also trigger self-assembly. Oscillating rheology of these mixtures (Supplementary Figure 1) revealed that the elastic modulus was

higher than the viscous modulus, confirming gel formation [23]. Furthermore, both SPA and HBPA formed stiffer gels with heparin sulfate than sodium hydroxide. We postulated that the polymeric nature of heparin sulfate contributed to this effect, either through formation of interfiber connections or by means of reinforcing the nanofibers themselves with intrafiber electrostatic bonds. Also, it can be noted that in general SPA formed stiffer gels than HBPA, with both its heparin-induced gel and its sodium hydroxide induced gel having a higher modulus than the comparable gels of HBPA. This is most likely due to a change in the nature of bundling of nanofibers caused by the altered sequence. It should be noted however that in general gels formed by the entanglement of these PA fibers are much weaker than other boil-derived gels like collagen which exhibit linear modulii in the range of 1.5–24.3 kPA depending on concentration. Hence while it is interesting that there is a statistically significant difference between the elastic modulii of the two types of PA gels, this does not translate to differences by orders of magnitude in stiffness, they are both within the same range of elastic modulus (G' between 10^1 –10^2 Pa).

Molecular interactions between SPA and heparin chains were studied in solution by ITC. In this technique a dilute solution of SPA is exposed to increasing amounts of dilute solutions of heparin and the heat associated with binding is measured. The data obtained was integrated and plotted against the molar ratio of the two molecules and a single-binding curve was fitted to obtain a binding constant of $2.82 \pm 0.1 \times 10^7$ (Figure 3). This is comparable with the binding constant of $1.1 \pm 0.03 \times 10^7$ previously obtained from a HBPA-heparin solution using the same technique [13]. The binding constant is also similar to that reported for other synthetic heparin binding peptides and heparin [24] but with one important difference. Previous studies have been able to obtain strong heparin affinity only by synthesizing polypeptides containing multiple repeats of the heparin binding sequence. In fact, peptides with a single consensus motif have been shown to have very poor affinity for heparin. In this study each molecule has only one motif and furthermore in the case of the SPA molecule the consensus sequence has been purposefully altered. It is interesting that it still exhibits a high degree of affinity. Since these molecules have been designed to self-assemble into nanofibers, we believe it is the self-assembly of PA monomers presenting the heparin binding peptide motifs at van der Waals density on the surfaces of the aggregates that explains the strong affinity observed in our systems. ITC was also used to obtain complete thermodynamic characterization of the binding event, including the Gibbs free energy change (ΔG), the enthalpy change (ΔH) and entropy change of the interaction (ΔS) [25,26]. Despite similarity in their binding constants, the binding interaction of HBPA and SPA differed in that the HBPA-heparin interaction was predominantly driven by entropic changes whereas the SPA-heparin interaction is predominantly enthalpic (Figure 3). This can be explained by their respective structures. HBPA has hydrophobic residues on the terminus of the peptide and the increase in entropy is possibly due to displacement of solvent water molecules from these residues upon heparin interaction. SPA, on the other hand, has charged basic residues on its terminus leading to strong electrostatic forces with the negatively charged heparin, and hence the predominance of binding enthalpy in its interactions with the biopolymer. An alternative explanation of the decreased entropy seen in the SPA-heparin interaction would be that there is less supramolecular aggregation of SPA molecules as compared to HBPA molecules upon the addition of heparin. This is less likely due to the following reasons. Previous work has shown that a single consensus sequence on a peptide chain is not sufficient to exhibit any measurable affinity to heparin [24]. In fact, only when a single molecule had three or more consensus sequences did it exhibit a similar degree of affinity to heparin by ITC as obtained here with SPA heparin interaction. In this case, not only does the SPA molecule have a single consensus motif, it has further been scrambled and yet it exhibits a high degree of affinity to heparin. This supports the presence of supramolecular aggregation of the SPA molecules under the conditions at which ITC measurements are being taken. This is further confirmed by circular dichroism data (CD), which shows a change in the spectrum from a predominantly α helix with SPA alone to a

predominantly β sheet conformation with the addition of heparin (Figure 3). This spectroscopic change was also seen previously with HBPA and heparin [13]. We have also previously established that β sheet formation is characteristic of self-assembly of PA monomers into nanofibers [14].

In order to study PA heparin interaction in the gelled state, two fluorescent confocal microscopic techniques were used- FRET and FRAP. FRET experiments were carried out using cylindrical SPA nanostructures doped with a donor fluorophore PA described previously [27] and using fluorescein-tagged heparin as an acceptor. The SPA nanostructures were coassembled with the donor fluorophore PA, and gels were formed using phosphate ions. These gels were suspended in solutions of fluorescein-tagged heparin and imaged using confocal microscopy. FRET experiments involved photobleaching of the acceptor (fluorescein-conjugated heparin) in a region of gel and monitoring of the percentage recovery of the donor fluorescence in that area (Figure 4). A FRET efficiency, which is directly proportional to the percentage recovery, was calculated using previously published methods [19] and found to be 0.81. This high efficiency indicates a close association between the two molecules (within 10 nanometers) [19] and is comparable to that measured in HBPA nanostructures interacting with fluorescein-conjugated heparin. In contrast, when the experiments were repeated with the donor fluorophore PA coassembled with a previously described control PA molecule with a negatively charged peptide sequence not expected to bind to heparin ($V_3A_3E_3$) , the FRET efficiency observed was significantly less (0.63, $p<0.05$) [27].

We used fluorescence recovery after photobleaching (FRAP) in order to study the kinetics of interaction between the two PA nanostructures (HBPA and SPA) and heparin in the gel state. Fluorescein-tagged heparin solution was added to either HBPA or SPA solutions to form fluorescent gels, and the gel fragments were imaged by fluorescent confocal microscopy. The fluorescein tagged to heparin was photobleached in an area and the recovery of fluorescence was monitored over time in that area. Since the fluorescein-heparin is irreversibly photobleached, any recovery in the area is due to diffusion of unbleached fluorescein heparin, either free or bound to one or more PA fibers, from neighboring areas. Hence, this is influenced by both heparin diffusivity and the binding strength of fluorescein-conjugated heparin with HBPA or SPA molecules in the respective gels. Multiple spots were photobleached to generate an average recovery curve, which was normalized both for imaging related photobleaching and for its pre-bleaching intensity to obtain recovery curves (Figure 5). From these curves, one can determine the mobile (or unbound) fraction of fluorescein conjugated-heparin using previously described methods [20]. It is interesting that this mobile fraction was significantly higher when measured in SPA-heparin gels compared to HBPA heparin gels (0.36 and 0.17 respectively, $p<0.05$). Furthermore, analysis of the data was performed as described previously by fitting a single binding site curve [21] to obtain the dissociation rate constant (k_{off}). The dissociation rate constant or k_{off} is the rate of the reverse unbinding reaction between the two interacting molecules [21]. In the SPA gel k_{off} was 1.7 times faster ($p<0.05$) than in the HBPA gel ($9.58 +/- 3 \times 10^{-5}$ s^{-1} and $5.52 +/- 0.9 \times 10^{-5}$ s^{-1} respectively). The nanofibers of an HBPA gel can be considered to provide surfaces on which heparin chains can be adsorbed. Theories of surface polymer adsorption have generated three types of contacts-a train where all the ‘mers’ are in contact with the surface, ‘loops’ which are unbound portions connecting the train ends on the surface and finally ‘tails’, unadsorbed polymer chain ends [28]. In this case also, since different parts of the heparin chain have a different sulfation pattern and since it is known that typical sulfation patterns determine affinity to heparin ligands, heparin is probably adopting a combination of trains, loops and tails on nanofiber surfaces, at times even bridging more than one nanofiber. Furthermore, it is known that it is more difficult to remove polymer chains than it is to attach them [28]. This is because there are multiple points of attachment to the surface and hence removing them needs several noncovalent bonds to be broken simultaneously [28]. Hence the overall kinetics of debonding is much slower than that

of initial bonding. It is interesting that SPA, which has a predominance of basic residues on the periphery of the nanofiber has a higher dissociation rate implying an overall lower debonding energy requirement than the HBPA. This suggests a role for the presence of the consensus sequence or the hydrophobic residues which are a part of it in the HBPA molecules stabilizing the electrostatic interaction with heparin. In fact, it is known that heparin chains form a high energy kink when interacting with the heparin binding domains of naturally occurring proteins [2]. This kink has been shown to consist of basic residues which are spaced apart from each other, either by means of hydrophobic residues in a linear sequence or by means of protein folding which brings together non-contiguous basic residues [2,18]. This high energy kink of the heparin chain is thought to be stabilized by van der Waals forces and ionic contact energy [2]. Hence, it is reasonable to conclude that it would require higher energy for heparin debonding from HBPA which has the consensus sequence compared to the SPA which has a cluster of basic residues on the periphery of the nanofiber. A specific role for the consensus sequence in heparin interaction is further supported by previous work using a sequence from antithrombin III, a protein which is known to interact with a pentasaccharide on heparin with a particular pattern of sulfation [29]. It was found that disrupting the consensus sequence while retaining the basic residues resulted in non-specific binding to all pentasaccharide sequences within heparin and not just the naturally occurring heparin binding one [29]. Finally, it has also been shown that the dissociation rate constant of a scrambled non-consensus heparin binding sequence was found to be higher when compared to the native heparin binding sequence found in amyloid P protein [30]. In summary, the interactions of heparin binding peptides with heparin are highly specific noncovalent ones that are sensitive to changes in peptide sequence. This is consistent with our observations here that scrambling of the consensus sequence increases the dissociation rate constant of heparin from the supramolecular nanofibers.

In order to establish if there was any effect on the bioactivity of the heparin when presented in a SPA vs. an HBPA gel we set up an in vitro angiogenesis assay using endothelial cells—the cell sandwich assay [31]. This is a well-known assay in which the ability of the material to induce sandwiched endothelial cells to re-organize into tubular structures is indicative of its angiogenic potential. In this assay bovine pulmonary arterial endothelial cells are sandwiched between two layers of SPA-heparin gel or HBPA-heparin gel with and without 25 ng of angiogenic heparin binding growth factors, fibroblast growth factor 2 (FGF-2) and vascular endothelial growth factor (VEGF). These cell cultures were followed up with alternate day media changes for seven days. We found that the cells grew in sheets in three dimensions with rare slit-like lumens and tubular structures seen at the end of seven days in both types of SPA-heparin gels without and with growth factors (Figure 6). In contrast, the HBPA-heparin gels with similar amounts of growth factors, exhibited tubule formation as early as day one and produced profuse tubular structures in three dimensions with continuous lumens by day seven (Figure 6). The HBPA gels without growth factor started showing some branching at day 3, and at day 7, these gels had tubules similar to the ones observed in the heparin binding gels with growth factors though smaller in number. Continuous tubule networks were only observed in gels formed by the HBPA fiber-heparin complex and not with the SPA-heparin gels. The tubules that were formed were quantified by manually tracing their length using imaging software (Supplementary Figure 2). This quantification revealed that the average tubule formation was statistically lower in SPA-heparin gels with (227 +/− 143 μms) and without growth factors (318.99 +/− 162.08 μms) as compared to the HBPA-heparin gels with growth factors (852 +/− 262 μms, $p<<0.01$ in each case). Furthermore, the HBPA-heparin gels without growth factors also had statistically lower tubular structure length (398.84 +/−242.05 μms, $p=0.01$) as compared to the HBPA- heparin gels with growth factors, though qualitatively the tubules in both types of gels appeared very similar. The presence of tubules of a remarkable degree of organization in the HBPA- heparin gels without growth factors can be explained by the fact that endogenous growth factors being secreted by the cells themselves are probably being activated and presented to them by the HBPA heparin matrix. Presence of supplemental

growth factors did not seem to play a role in tubule formation in the SPA-heparin gels. In the case of the SPA-heparin gels, absence of the consensus sequences seems to alter the interaction with heparin in such a way as to decrease its bioactivity, even in the presence of supplemental growth factors. From the FRAP results, it is known that both the mobile fraction of heparin and the dissociation rate constant of heparin is higher in SPA gels. This higher molecular turnover of heparin in a SPA gel could be a reason for the decreased bioactivity seen in the *in vitro* angiogenesis assay as compared to the HBPA-heparin gel. As discussed above, it is known that the consensus sequence often seen in heparin binding portions of naturally occurring proteins stabilize the interaction with heparin [2,18]. In fact, naturally occurring heparin binding proteins are not known to exhibit a series of contiguous basic residues even in their heparin binding portions [18]. The stability obtained from non-electrostatic interactions may be essential for the participation of heparin in biological signaling. In the case of SPA molecules, since basic residues are clustered on the periphery of the nanofiber, their interaction with heparin is predominantly driven by electrostatic attraction and mechanisms discussed above do not come into play thus leading to decreased bioactivity. We propose that the presentation of heparin chain segments on the HBPA nanofibers is optimal for cell signaling (schematic shown in Figure 7). The presence of a large surface area of noncovalently coated heparin with optimal conformation might be able to activate efficiently, growth factors on the nanofibers, thus promoting tubule formation.

Conclusions

We have shown that heparin triggers self-assembly of a peptide amphiphile with a concensus amino acid sequence inspired by the heparin binding domains of proteins (HBPA) but also of one in which this peptide sequence is scrambled (SPA). Even though both PAs form nanofibers upon mixing with heparin and have also similar binding constants with this polysaccharide, there are important differences in the nature of their interaction. In solution, the interaction between heparin and HBPA seems to be driven predominantly by changes in entropy, possibly due to displacement of water, whereas the heparin-SPA interaction is predominantly enthalpic and could be based on electrostastic interactions. In the gel state, a high FRET efficiency shows the proximity of heparin molecules to both HBPA and SPA molecules, indicating a close association between the polymer and the peptide amphiphiles. However, the kinetics of interaction is different between the two with a larger dissociation rate constant and a larger mobile fraction in SPA-heparin gels, as demonstrated by FRAP experiments. While HBPA and SPA have similar affinities for heparin, SPA has a faster off rate with heparin leading to a higher turnover of heparin molecules on the nanostructures and an increased mobile or unbound fraction of the biopolymer. Interestingly, these differences seem to decrease the bioactivity of heparin based on an in vitro angiogenesis assay relative to the consensus sequence. We suggest that the conformation of heparin on nanostructures displaying the consensus sequence of the HBPA molecules is optimal for bioactivity, and that heparin binding to synthetic peptides and the consequent interaction with proteins is highly specific.

Supplementary Material

Refer to Web version on PubMed Central for supplementary material.

Acknowledgements

This work was funded by the National Institutes of Health (1R01 EB003806-04) and the U.S. Army Telemedicine and Advanced Technology Research Center (TATRC W81XWH-05-1-0381). We thank Dr. B.M. Rabatic for performing the TEM, Dr. M. S. Rao for assistance with the CD and oscillating rheometry and Dr W. Lowe Jr. from the Department of Medicine at Northwestern University Feinberg School of Medicine, for donating the bPAEC. We also thank the following facilities at Northwestern University - the Biological Imaging Facility and the Cell Imaging

Facility, the Keck Biophysics Facility, the Electron Probe Instrumentation Center, the Analytical Services Laboratory and Prof. W. R. Burghardt for use of the oscillating rheometer.

References

1. Varki, A.; Cummings, R.; Esko, J.; Freeze, H.; Hart, G.; Marth, J. Essentials of Glycobiology. 1 ed. Plainview, NY: Cold Spring Harbor Laboratory Press; 1999.
2. Raman R, Sasisekharan V, Sasisekharan R. Structural insights into biological roles of protein-glycosaminoglycan interactions. Chemistry & Biology 2005 Mar;12(3):267–277. [PubMed: 15797210]
3. Tyrell DJ, Kilfeather S, Page CP. Therapeutic uses of heparin beyond its traditional role as an anticoagulant. Trends Pharmacol Sci 1995;16:198–204. [PubMed: 7652929]
4. Sasisekharan R, Shriver Z, Venkataraman G, Narayanasami U. Roles of Heparan-Sulphate Glycosaminoglycans in Cancer. Nat Rev Cancer 2002;2:521–528. [PubMed: 12094238]
5. Osmond RIW, Kett WC, Skett SE, Coombe DR. Protein-heparin interactions measured by BIAcore 2000 are affected by the method of heparin immobilization. Analytical Biochemistry 2002 Nov;310 (2):199–207. [PubMed: 12423639]
6. Schlessinger J, Plotnikov AN, Ibrahimi OA, Eliseenkova AV, Yeh BK, Yayon A, et al. Crystal structure of a ternary FGF-FGFR-heparin complex reveals a dual role for heparin in FGFR binding and dimerization. Molecular Cell 2000;6(3):743–750. [PubMed: 11030354]
7. Keyt BA, Berleau LT, Nguyen HV, Chen H, Heinsohn H, Vandlen R, et al. The carboxyl-terminal domain (111-165) of vascular endothelial growth factor is critical for its mitogenic potency. J Biol Chem 1996;271(13):7788–7795. [PubMed: 8631822]
8. Cardin AD, Weintraub HJR. Molecular Modeling of Protein-Glycosaminoglycan Interactions. Arteriosclerosis 1989 Jan–Feb;9(1):21–32. [PubMed: 2463827]
9. Healy KE, Rezania A, Stile RA. Designing biomaterials to direct biological responses. Bioartificial Organs Ii: Technology, Medicine, and Materials 1999:24–35.
10. Sakiyama-Elbert SE, Hubbell JA. Controlled release of nerve growth factor from a heparin-containing fibrin-based cell ingrowth matrix. Journal of Controlled Release 2000 Oct;69(1):149–158. [PubMed: 11018553]
11. Delucia A, Wakefield TW, Andrews PC, Nichol BJ, Kadell AM, Wrobleski SK, et al. Efficacy and Toxicity of Differently Charged Polycationic Protamine-Like Peptides for Heparin Anticoagulation Reversal. Journal of Vascular Surgery 1993 Jul;18(1):49–60. [PubMed: 8326659]
12. Schick BP, Maslow D, Moshinski A, Antonio JDS. Novel concatameric heparin-binding peptides reverse heparin and low-molecular-weight heparin anticoagulant activities in patient plasma in vitro and in rats in vivo. Blood 2004;103:1356–1363. [PubMed: 14576044]
13. Rajangam K, Behanna HA, Hui MJ, Han X, Hulvat JF, Lomasney JW, et al. Heparin binding nanostructures to promote growth of blood vessels. Nano Lett 2006;13:2086–2090. [PubMed: 16968030]
14. Behanna HA, Donners JJM, Gordon AC, Stupp SI. Coassembly of Amphiphiles with Opposite Peptide Polarities into Nanofibers. J Am Chem Soc 2005;127:1193–1200. [PubMed: 15669858]
15. Hartgerink JD, Beniash E, Stupp SI. Self-assembly and mineralization of peptide-amphiphile nanofibers. Science 2001;294(5547):1684–1688. [PubMed: 11721046]
16. Hartgerink JD, Beniash E, Stupp SI. Peptide-amphiphile nanofibers: A versatile scaffold for the preparation of self-assembling materials. Proc Nat Acad Sc USA 2002;99(8):5133–5138. [PubMed: 11929981]
17. Silva GA, Czeisler C, Niece KL, Beniash E, Harrington DA, Kessler JA, et al. Selective Differentiation of Neural Progenitor Cells by High-Epitope Density Nanofibers. Science 2004;303(5662):1352–1355. [PubMed: 14739465]
18. Hileman RE, Fromm JR, Weiler JM, Linhardt RJ. Glycosaminoglycan-protein interactions: definition of consensus sites in glycosaminoglycan binding proteins. Bioessays 1998;20:156–167. [PubMed: 9631661]
19. Nerney C, Danuser G. FRET or no FRET: A quantitative comparison. Biophys J 2003;84:3992. [PubMed: 12770904]

20. Lippincott-Scwartz J, Snap E, Kenworthy A. Studying Protein Dynamics in Living Cells. Nat Rev Mol cell Biol 2001;2:444–456. [PubMed: 11389468]
21. Sprague BL, Pego RL, Stavreva DA, McNally JG. Analysis of binding reactions by fluorescence recovery after photobleaching. Biophysical Journal 2004 Jun;86(6):3473–3495. [PubMed: 15189848]
22. Paramonov SE, Jun H-W, Hartgerink JD. Self-Assembly of Peptide-Amphiphile Nanofibers: The Roles of Hydrogen Bonding and Amphiphile Packing. J Am Chem Soc 2006;128(22):7291–7298. [PubMed: 16734483]
23. Ross-Murphy SB, Shatwell KP. Polysaccharide Strong and Weak Gels. Biorheology 1993;30:217. [PubMed: 8286724]
24. Verrecchio A, Germann MW, Schick BP, Kung B, Twardowski T, San Antonio JD. Design of peptides with high affinities for heparin and endothelial cell proteoglycans. J Biol Chem 2000;275(11):7701–7707. [PubMed: 10713081]
25. Cooper A. Thermodynamic analysis of biomolecular interactions. Current Opinion in Chemical Biology 1999 Oct;3(5):557–563. [PubMed: 10508661]
26. Holdgate GA. Making cool drugs hot: Isothermal titration calorimetry as a tool to study binding energetics. Biotechniques 2001 Jul;31(1)164-+
27. Behanna HA, Rajangam K, Stupp SI. Modulation of fluorescence through co-assembly of molecules in organic nanostructures. J Am Chem Soc 2007;129:321–327. [PubMed: 17212411]
28. Sperling, LH. Introduction to physical polymer science. 3 ed. Wiley-Interscience; 2001.
29. Bae J, Desai UR, Pervin A, Caldwell EE, Weiler JM, Linhardt RJ. Interaction of heparin with synthetic antithrombin III peptide analogues. Biochem J 1994;301:121–129. [PubMed: 8037658]
30. Hernaiz MJ, LeBrun LA, Wu Y, Sen JW, Linhardt RJ, Heegaard NHH. Characterization of heparin binding by a peptide from amyloid P component using capillary electrophoresis, surface plasmon resonance and isothermal titration calorimetry. European Journal of Biochemistry 2002 Jun;269(12):2860–2867. [PubMed: 12071948]
31. Montesano R, Orci L, Vassalli P. Invitro Rapid Organization of Endothelial-Cells into Capillary-Like Networks Is Promoted by Collagen Matrices. J of Cell Biol 1983;97(5):1648–1652. [PubMed: 6630296]

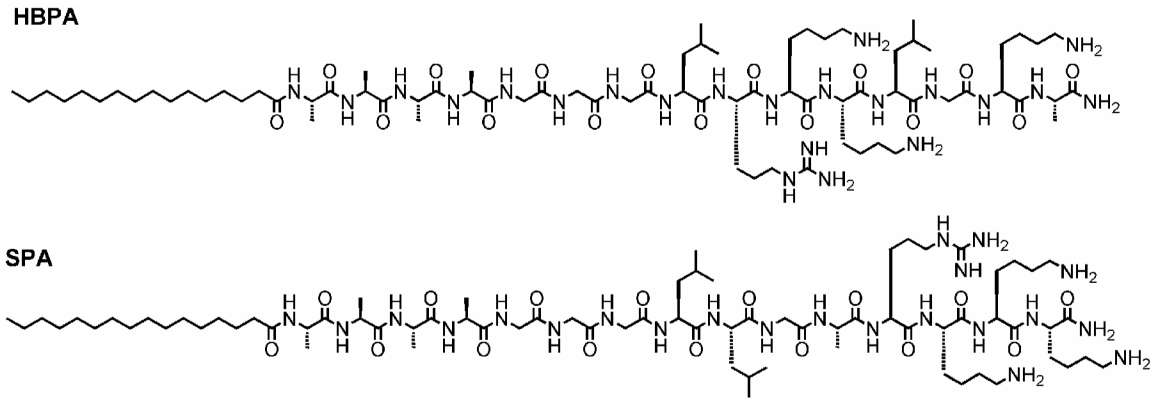

Figure 1.
Molecular structures of the peptide amphiphiles

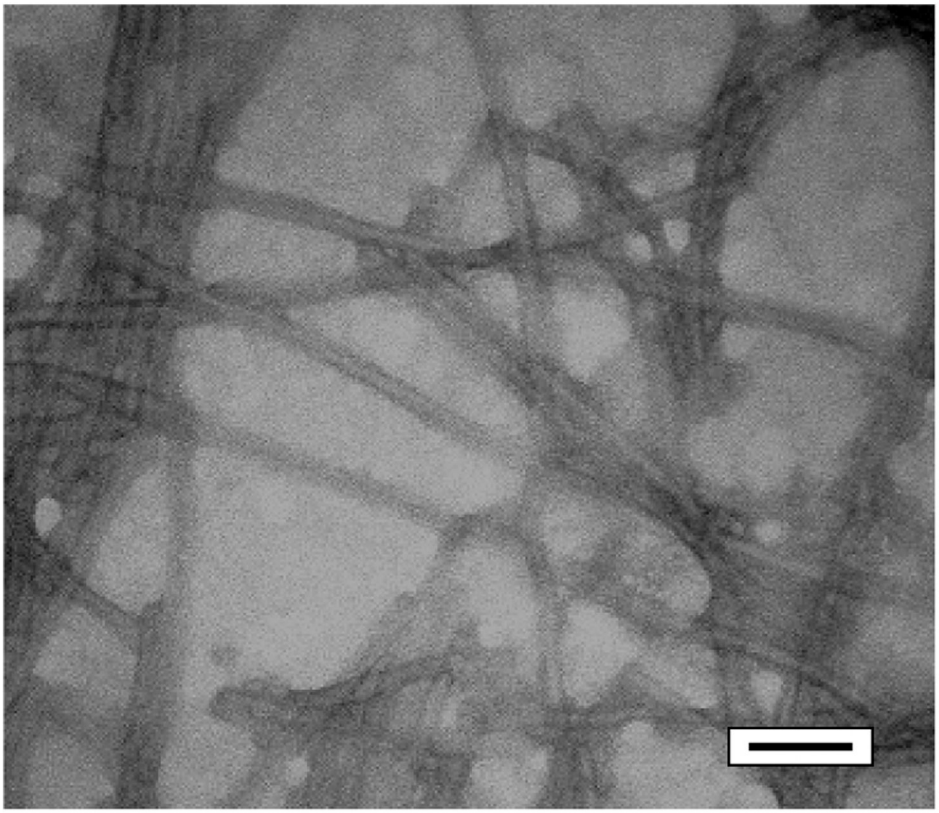

Figure 2.
TEM. Micrograph of SPA heparin gel showing bundles of nanofibers stained with phosphotungstic acid (scale bar = 50 nanometers)

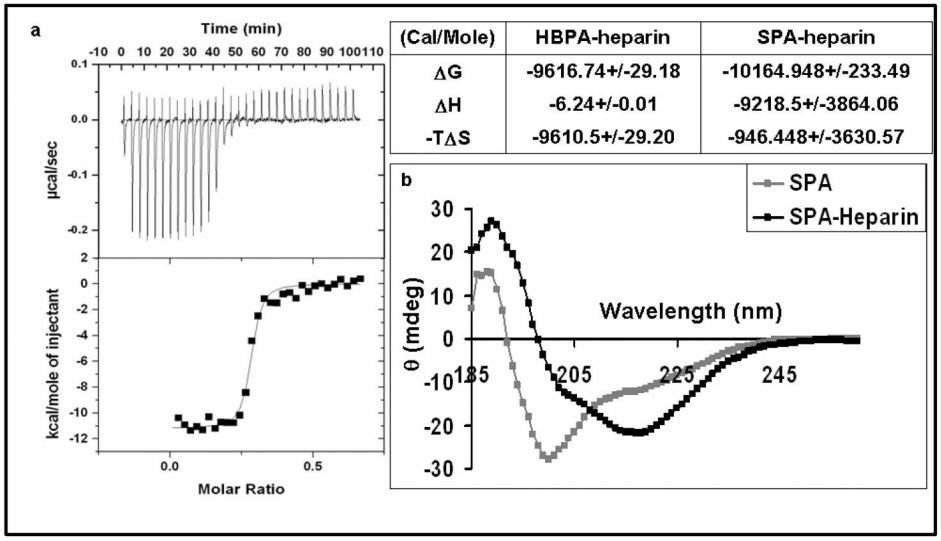

Figure 3.

SPA-heparin interactions in solution. 3a is isothermal titration calorimetry graphs showing the heat released upon addition of heparin into SPA in solution with the integrated values (black dots) and the fit line (black line) shown below. The table compares the thermodynamic signature of SPA heparin interaction with HBPA heparin interaction (values represent averages and 95% confidence intervals). Figure 3b plots CD spectra showing predominant β sheet formation for SPA in the presence of heparin (black) compared to predominantly α helix formation without heparin (grey). The SPA heparin spectra have been corrected for contribution by heparin alone.

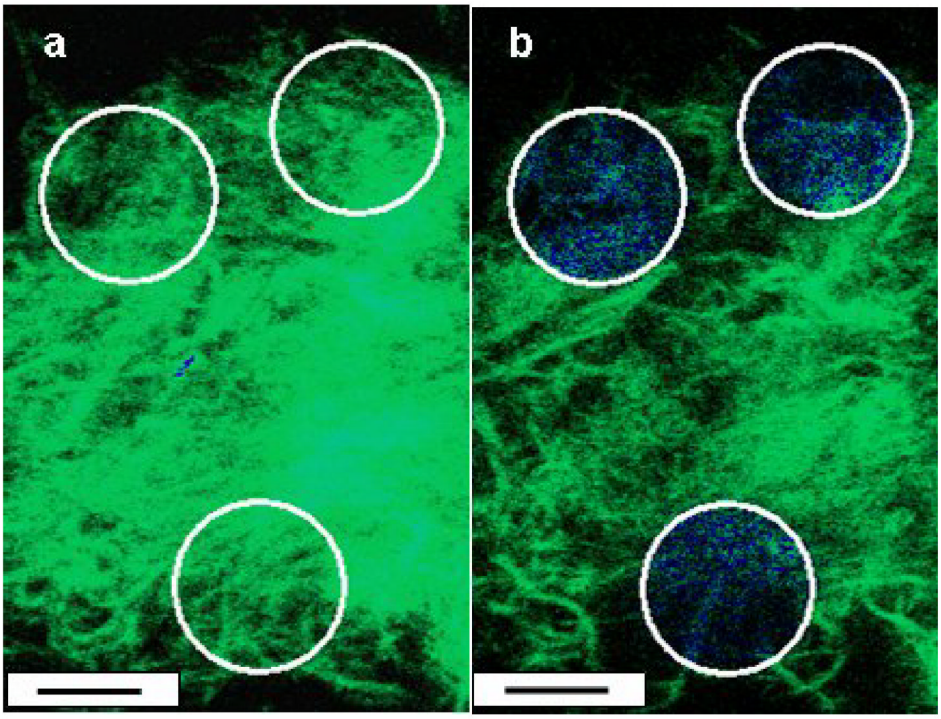

Figure 4.
FRET by acceptor photobleaching. Images of a gel formed by mixing SPA doped with a donor fluorophore and fluorescein tagged heparin (acceptor) before (a) and after (b) photobleaching of an area (white circle). The fluorescent emission of the donor (blue) recovers when the acceptor has been photobleached (scale bar= 10 μm). The respective FRET efficiencies for the two are 0.81 and 0.63 ($p < 0.05$).

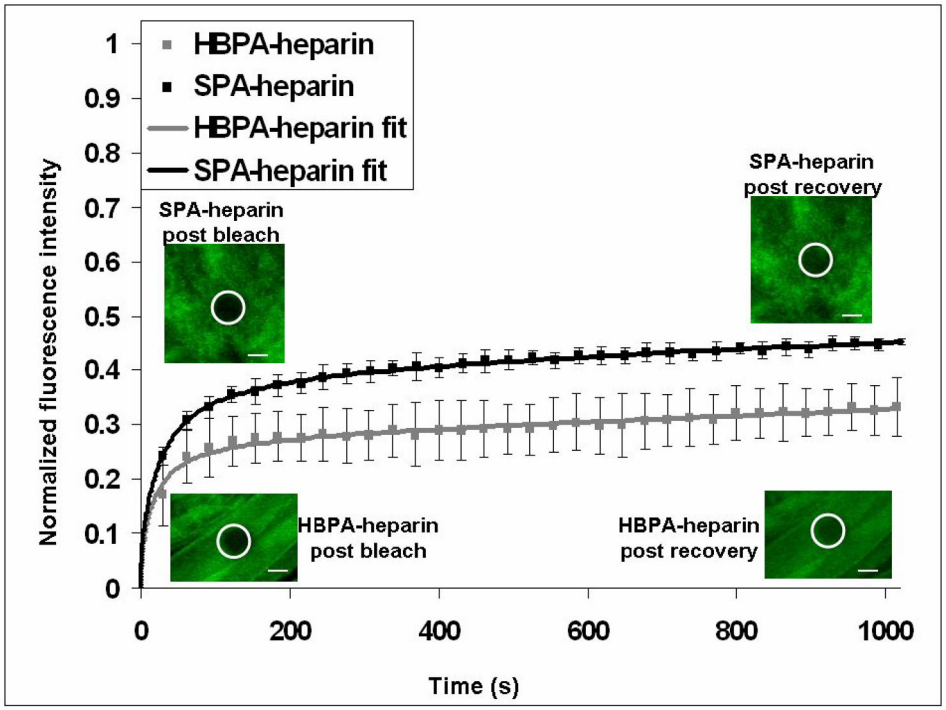

Figure 5.

FRAP. Graph plotting the normalized fluorescence in the photobleached areas (white circles in inset) showing higher mobile fraction in the SPA-heparin gels compared to the HBPA-heparin gels. A non linear, least squares fit assuming a single type of binding site (solid lines) was done to reveal a faster dissociation rate constant for heparin in SPA heparin gels compared to HBPA heparin gels (values shown are averages and 95% confidence levels, scale bars in inset 5 μm)˜.

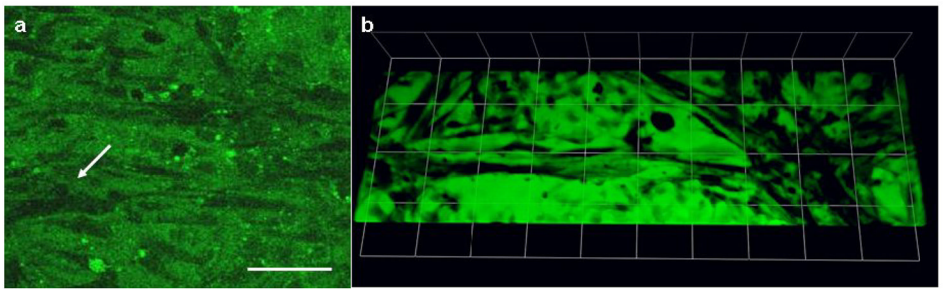

Figure 6.
In vitro angiogenesis assay. Confocal fluorescent micrographs of bPAEC stained with vybrant CFDA seven days after cell sandwich show occasional slit like lumen in SPA heparin gels with growth factors (a) (scale bars = 80 μm) and profuse interconnected tubular structures in HBPA gels with growth factors (b) (each side of grid= 75 μm).

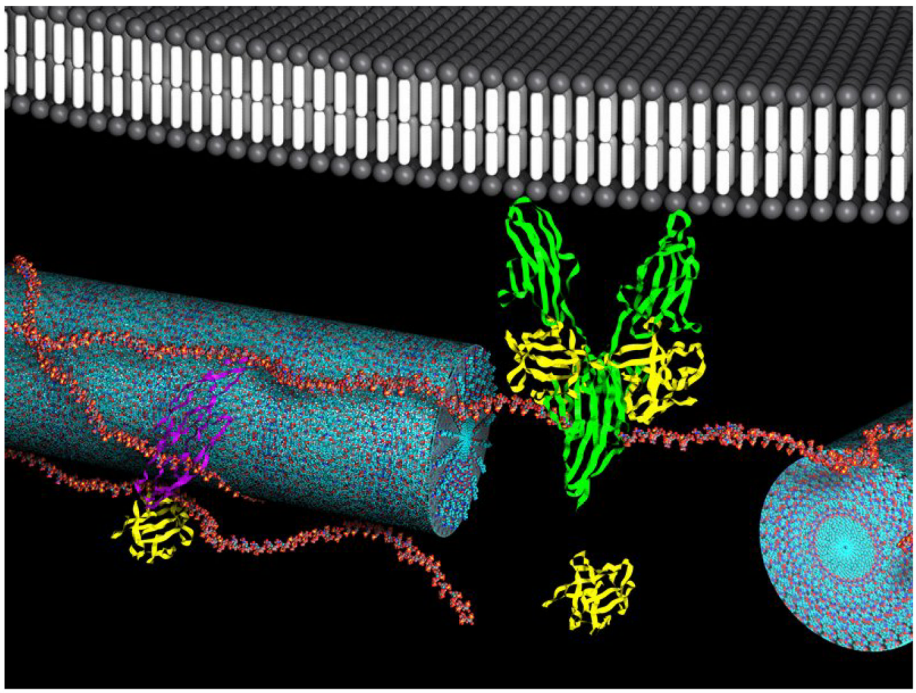

Figure 7.
Schematic representation of heparin-nucleated HBPA nanofibers interacting with GF and receptors. The HBPA nanofibers (blue) are shown with adsorbed heparin chains on them (red). Heparin is known to bind and activate VEGF (purple), FGF-2 (yellow) and FGF-receptor (green). The schematic proposes that the heparin-FGF-2-FGF receptor complex is further stabilized by their anchoring on HBPA nanofibers. It is possible that the absence of heparin stabilization by hydrophobic interactions and the consensus format in the SPA nanofibers is responsible for the decreased bioactivity seen in SPA heparin gels.